Journal of
Applied Crystallography

ISSN 0021-8898

Received 16 March 2007
Accepted 4 June 2007

Modelling of diffraction from fibre texture gradients in thin polycrystalline films

M. Birkholz

IHP, Im Technologiepark 25, 15236 Frankfurt (Oder), Germany. Correspondence e-mail: birkholz@ihp-microelectronics.com

Crystallographic textures in thin polycrystalline films typically exhibit a rotational symmetry, *i.e.* they occur as a fibre texture with the texture pole being orientated in the direction of the substrate normal. As a further characteristic of thin-film textures, it was often observed that the degree of preferred orientation increases with increasing thickness. It is shown in this work how a fibre texture gradient may be modelled in kinematical X-ray diffraction and which effects it has on the intensity mapping of the I_{HKL} reflection, when the HKL pole is the fibre axis. A general expression for I_{HKL} is derived for a depth-dependent fibre texture that is based on the finite Laplace transform of the texture distribution. The concept is outlined for the $\cos^n\psi$ function to model the tilt-angle dependence of intensity, with the parameter n denoting the degree of texture. It is found that the measured intensity distribution sensitively depends on the ratio of texture gradient over X-ray attenuation coefficient. For particular cases, it is found that the maximum intensity may occur for non-zero tilt angles and thus arise at a different tilt angle from the pole of the fibre texture.

1. Introduction

Modern technological devices to a large extent rely on thin polycrystalline films having a thickness between a few and some thousands of nanometres. This holds for instance for integrated circuits from the semiconductor industry, sensoric layers, optical systems, protective and resistive coatings on food wrappings, turbine engines and cutting tools, to mention only a few examples (Ohring, 2002). Often, thin polycrystalline films exhibit a pronounced preferred crystallographic orientation or texture, with one particular lattice plane (HKL) preferentially oriented parallel to the substrate. The effect is most strongly revealed in X-ray powder diffraction patterns, where the intensity of the Bragg reflection HKL of the preferred plane exceeds all other reflections. In addition, inorganic layers are often found to exhibit a fibre texture or layer texture (Birkholz, 2006), *i.e.* the orientation distribution function (ODF) of crystallites is rotationally symmetric with respect to the substrate normal $\mathbf{s}_3$. In the case of metals, for instance, face-centred cubic (f.c.c.) structures are often found to yield a ⟨111⟩ fibre texture, whereas diamond-structured semiconductors exhibit a ⟨110⟩ or ⟨100⟩ fibre depending on the deposition temperature (Wenk *et al.*, 1990). A proper understanding of thin-film textures, and advantageously their tailoring on demand, is a highly relevant question, since the anisotropy of physical properties is mapped *via* the ODF into the functioning of the device (Bunge, 1969, 1982; Wenk & van Houtte, 2004). The relevance of this statement is emphasized by pyro-, ferro- and piezoelectric layers, for which the polar axis has to be adjusted to a given direction with respect to the substrate reference frame (Chateigner, 2000). In particular, the nearly perfect alignment of crystallographic c axes along the substrate normal in polycrystalline wurtzite-structured thin films is the decisive structural presupposition for their application as transparent electrodes (Birkholz *et al.*, 2003) or in surface acoustic wave (SAW) devices (Caliendo & Imperatori, 2004). The latter application is currently under investigation for fully CMOS-integrated biomolecular sensors that would operate without an optical label of the analyte.

It turned out during a large number of thin-film studies that a fibre texture often evolves with increasing layer thickness, tempting one early researcher of the phenomenon to denote it as an evolutionary process (van der Drift, 1967). The physical causes behind these processes are still under discussion (Kajikawa *et al.*, 2003; Kajikawa, 2006). It has been argued that they are due to differences in crystal growth velocities (van der Drift, 1967; Fenske *et al.*, 2005), induced by ion implantation and channelling (Rauschenbach & Helming, 1989), minimization of elastic deformation energy (Pelleg *et al.*, 1991) or surface energy (Fujimura *et al.*, 1993; Knuyt *et al.*, 1996), ion-induced damage and subsequent recrystallization (Dong & Srolovitz, 1999), preferential etching by reactive gas phase species (Kamiya *et al.*, 1999; Birkholz *et al.*, 2000), surface coverage of reactive gas atoms (Shin *et al.*, 2002), the combined effects of alloying and annealing (Platt *et al.*, 2002), plastic deformation by ion bombardment (Birkholz *et al.*, 2004), and other sources. It has to be stated, however, that only few experimental studies revealed a full quantitative description of the texture's thickness dependence. From a thin-film grower's point of view, it would be reliable to assume

that the details of a texture gradient depend on the precise nature of the deposition process, being either electroplating, spin coating, physical or chemical vapour deposition *etc*., and their operational characteristics, such as deposition temperature, pressure, growth rate, particle and charged particle fluxes, *etc*. Indeed, it cannot be excluded that the various mechanisms are active concomitantly, and it can be expected that different texture gradients may be elicited by choosing a particular deposition process. This all emphasizes the necessity for experimental studies that thoroughly and quantitatively account for the phenomenon.

It is intriguing to compare the state of knowledge to that in the field of residual stress, which represents another important microstructural property of thin solid films. There, a comprehensive approach for measuring and analysing residual stress gradients has been developed in the framework of the scattering vector technique (Genzel, 1999, 2004; Genzel *et al.*, 1999). The analysis of residual stress gradients in thin films has proven its significance to elucidate the mechanisms of microstructure formation, as has recently been shown, for instance, in the case of nitride hard coatings (Genzel & Reimers, 2003; Göbel *et al.*, 2001) and thin metallic layers, the latter of which were subjected to an intense ion bombardment during growth (Birkholz *et al.*, 2004). In addition, the question of residual stress in the presence of sharp textures has already been tackled (Baron & Hauk, 1988; Genzel, 1998; Genzel & Reimers, 1998; Saerens *et al.*, 2000; Popa & Balzar, 2001; Scardi & Dong, 2001; Almer *et al.*, 2003; Welzel & Mittemeijer, 2003).

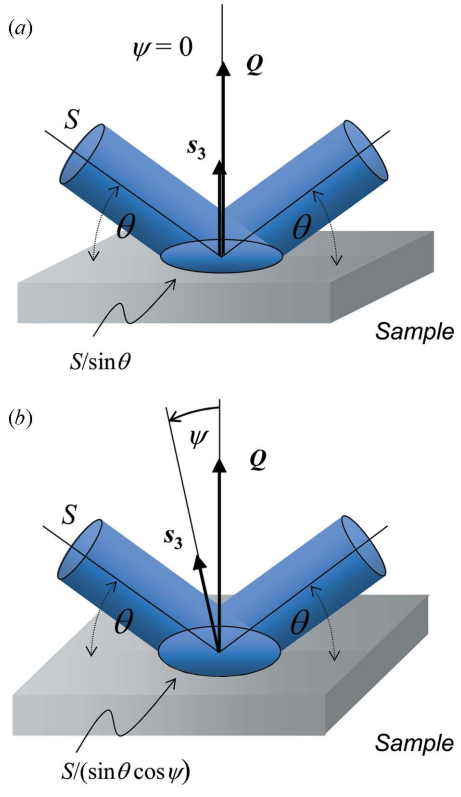

Figure 1
Illuminated sample areas for an X-ray beam of area S in a symmetrical $\theta/2\theta$ scan (a) with zero tilt angle ψ, $S \rightarrow S/\sin\theta$, and ($b$) for $\psi \neq 0$, $S \rightarrow S/(\sin\theta\cos\psi)$.

What is missing in the actual discussion of possible stress–texture interactions, however, is a technique that allows the determination of texture gradients to verify or disprove the physical concepts that consider the one as the cause for the other. It might be expected that the simultaneous evaluation of stress and texture gradients will yield interesting insights into the mechanisms of thin-film growth.

This work will outline how texture gradients may be determined from a set of experimental diffraction data. Texture gradients have already been dealt with in a previous study, with emphasis on fully general three-dimensional ODFs as they are relevant for mechanical work pieces and plastic deformations by rolling processes, *etc*. (Bonarski *et al.*, 1998). The work presented here will focus on the evolution of fibre textures in thin solid films in the direction of the substrate normal. Compared with the classical texture analysis of polycrystalline samples, two further steps of sophistication will be employed that account for the inclusion of finite sample thickness and the gradation of texture. A central point of this work is the generalization of the formula of Bragg reflection intensity in the kinematic approximation for these improved levels of sophistication. It is hoped that *via* the application of the method, the sparse database of fibre texture gradients may be extended in order to place the theoretical modelling of this interesting evolutional process on a firm experimental basis.

2. Modelling of tilt-angle dependence

A layer texture can be described by an orientation distribution function $T_{\rm H}(\psi)$ accounting for the concentration of preferentially oriented lattice planes (HKL) or **H** as a function of inclination ψ. The latter measures the angle between the substrate normal $\mathbf{s}_3$ and the lattice plane normal **H** or the scattering vector **Q**; see Fig. 1. The distribution function of the fibre reflection $T_{\rm H}(\psi)$ or any other reflection $T_{\rm h}(\psi)$ can be determined by X-ray diffraction procedures, where the intensity of a Bragg reflection is measured in the symmetric $\theta/2\theta$ mode for successive tilt angles ψ. In the kinematic approximation, the integral intensity of a homogeneous, polycrystalline specimen as a function of tilt angle ψ is of the form

$$I_{\rm h}(\psi) = {\rm SCF}'\,\lambda^3\,{\rm Lp}\,m_{\rm h}\,\left|F_{\rm h}\right|^2\,T_{\rm h}(\psi)\,V_{\rm sc} \qquad (1)$$

with $F_{\rm h}$, $m_{\rm h}$, Lp, and $V_{\rm sc}$ standing for the structure factor, multiplicity, Lorentz polarization factor of the reflection, and the scattering volume (Birkholz, 2006), respectively. SCF′ is an instrumental scaling factor depending on incoming intensity, goniometer radius, scanning speed and other non-sample-related quantities. It will be distinguished in the following in utilizing the subscript h for hkl or H for HKL. The latter should denote all quantities of fibre-textured lattice planes, while the first indicates a general validity for all lattice planes.

Most reliable data for fibre textures are obtained by collecting a set of symmetric $\theta/2\theta$ scans for different tilt angles ψ by use of an Euler cradle; see Fig. 1. In this measurement setup, the X-ray footprint on the sample, $Sk/2$, depends on the

beam area S and a configuration parameter k. In a $\theta/2\theta$ scan without inclining the sample, $k = 2/\sin\theta$ holds (Fig. 1*a*), while an inclination of the sample by angle ψ (Fig. 1*b*) causes the configuration factor to become

$$k = 2/(\sin\theta\cos\psi). \tag{2}$$

The configuration parameter may be understood as a multiplication factor by which the depth z has to be multiplied to obtain the X-ray path length 2ℓ within the sample for a beam scattered at depth z. The intensity distribution $I_h(\psi)$ is measured by setting the goniometer to a set of fixed ψ values, performing $\theta/2\theta$ scans and determining the reflection intensity for each ψ.

The scattering volume V_{sc} in equation (1) may be expected to scale with the product of S and the beam's penetration depth or with S/μ, where μ is the linear X-ray attenuation coefficient. In the case of a thin film, the scattering volume will moreover depend on the thickness t. The precise value for V_{sc} is obtained by integrating over all incoming and exciting beams; see Fig. 1.15 of Birkholz (2006). For the integration in the beam direction, the substitution $\ell = zk/2$ and $\ell_{max} \rightarrow t$ has to be performed to adapt to the measurement geometry, resulting in the expression

$$V_{sc} = S\int_0^{\ell_{max}} \exp(-2\mu\ell)\,\mathrm{d}\ell = S\frac{k}{2}\int_0^{t} \exp(-\mu z k)\,\mathrm{d}z$$
$$= \frac{S}{2\mu}[1 - \exp(-\mu t k)]. \tag{3}$$

The resulting scattering volume may then be represented by multiplying $S/(2\mu)$ with an absorption factor $A(t)$ that depends on Bragg angle θ and inclination ψ according to

$$A(t) = 1 - \exp(-\mu t k). \tag{4}$$

Since the beam area S is constant throughout the scan, it may be included in SCF′ by changing to a modified scaling factor SCF = SSCF′ and one may write for the Bragg reflection intensity of a polycrystalline specimen of thickness t,

$$I_h(\psi, t) = \mathrm{SCF}\,\lambda^3\,\mathrm{Lp}\,m_h\,|F_h|^2\,T_h(\psi)\,\frac{1}{2\mu}\,A(t). \tag{5}$$

Depending on the type of experiment, the wavelength λ may also be included into the scaling factor. However, this has not been done here in order to allow for comparison of integral intensities measured with different X-ray wavelengths. Equation (5) gives the basis for the combined analysis approach, being an extended Rietveld analysis that not only allows the determination of lattice and positional parameters, but also of microstructural data such as crystallite size, texture, microstress and residual stress from a set of measured $\theta/2\theta$ scans at various tilt angles (Lutterotti *et al.*, 2004; Chateigner, 2005).

The decisive distinction in the integral intensity for a powder sample of assumingly infinite thickness and a polycrystalline thin film is represented by the absorption factor $A(t)$ or, equivalently, by the magnitude of the μt product. It can be realised from equation (4) that the transition between both cases is obtained for $t \rightarrow \infty$, making $A(t)$ approach unity. The majority of thin films of technological relevance will exhibit μt values between 10^{-5} and 1, causing $A(t)$ to become significantly less than unity and thus to diminish the scattering intensity. For illustration, Fig. 2 displays the variation of some μt values for representative thin-film materials of 1 µm thickness in the X-ray energy range between 5 and 15 keV. According to the layer's chemical composition, pronounced discontinuities arise at the energy of elemental absorption edges. It may well be expected that absorption will also affect the measurement of thin-film fibre texture and evidently the μt product will have to be included in the analysis.

A typical map of a set of $\theta/2\theta$ intensity scans under different inclinations from a wurtzite-structured thin ZnO:Al film measured with Cu $K\alpha$ is shown in Fig. 3. It is realised from the different I_{hkl} distributions in the $(2\theta, \psi)$ plane that this layer exhibits a pronounced ⟨00*l*⟩ texture; further details on this sample and its texture can be found in work by Birkholz *et al.* (2003) and Fenske *et al.* (2005). The intensity distribution $I_H(\psi, t)$ can be imagined to be derived from different sections

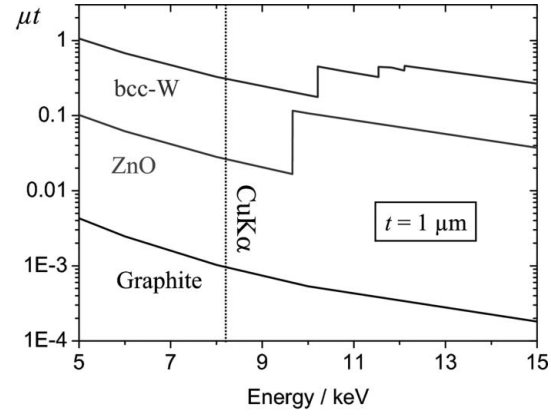

Figure 2
μt product functions of representative thin-film materials b.c.c. tungsten, hexagonal ZnO and graphite with high, average and low electron densities in the X-ray energy range between 5 and 15 keV. The film thickness t has been assumed to amount to 1 µm.

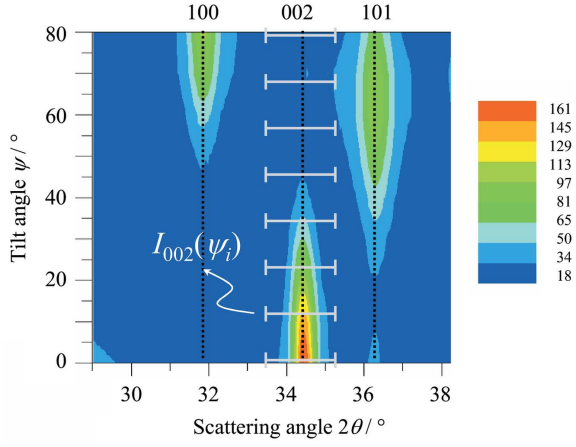

Figure 3
Intensity map $I_H(2\theta, \psi)$ of a nominally 500 nm ZnO:Al sample exhibiting a pronounced ⟨002⟩ fibre texture. The colour scale is in counts per second (cps). The light grey bars should indicate the set of $\theta/2\theta$ scans to be performed for a determination of the $I_H(\psi, t)$ distribution.

of one Bragg peak as visualized in the figure for the 002 reflection. It is evident that the integration over the full orientation distribution $T_h(\psi)$ should cover all crystallites in the illuminated sample volume. Because fibre textures are considered here, the integration over $T_h(\psi)$ does not depend on the azimuth and simply yields the constant 2π. The normalization of $T_h(\psi)$ is then performed according to

$$\int_0^{2\pi} d\varphi \int_0^{\pi/2} T_h(\psi) \sin\psi \, d\psi = 2\pi \int_0^{\pi/2} T_h(\psi) \sin\psi d\psi = 1. \quad (6)$$

It has to be emphasized that the upper limit of the tilt angle integration is $\pi/2$ instead of π as might have been expected at first thought. This has to be done, because two reflecting lattice planes **h** at ψ and $-\mathbf{h}$ at $\pi - \psi$ account for the same Bragg reflection and should not contribute twice to the intensity (which is already included in the multiplicity factor m_h). The approach is justified by Friedel's law and deserves modification if anomalous scattering from polar polycrystals has to be considered.

Various approaches have been tested to model the tilt-angle dependence of measured $T_H(\psi)$ distributions, such as: the so-called March function or March–Dollase function (March, 1932; Dollase, 1986[1]) that was initially developed for plastically deformed rocks and was found to generally apply to cylindrically shaped crystallites being either flat disks or elongated grains; or other monotonically decreasing functions with different numbers of free parameters and shapes (Dollase, 1986) being proportional to either $\exp(-\psi^2)$, $\exp(-n/\cos\psi)$, $\exp(-n^2/\cos^2\psi)$, or $\exp(-G/\cos^n\psi)$, *etc.*

Orthonormal sets from basis functions have also been applied, for example in Bunge's formulation of the harmonic texture analysis (Bunge, 1969, 1982), where a fibre texture is decomposed into a finite sum of normalized Legendre functions P_l,

$$T_h(\psi) = \sum_{l=0}^{l_{max}} c_l P_l(\cos\psi). \quad (7)$$

The expansion has to be truncated beyond a limiting order, yielding $l_{max} + 1$ coefficients c_l that stand for the weight of each component. The approximation of layer texture distributions by this expansion has the disadvantage that unreasonable oscillations from the P_l are introduced into the typically monotone course of T_H.

A simple and mathematically sound modelling of fibre texture intensity is given by the normalized $\cos^n\psi$ function

$$T_H(\psi) = N_n \cos^n \psi. \quad (8)$$

In this approach, the measured intensity distribution is accounted for by a single parameter, being the fibre texture degree n. For the modelling of measured $I_H(\psi, t)$ data, the order parameter n may assume any positive real number, while a value of $n = 0$ would account for a random distribution of crystallites. The normalization factor according to equation (6) becomes

$$N_n = \frac{n+1}{2\pi}. \quad (9)$$

A set of these texture distribution functions for various orders of n is given in Fig. 4 on a linear (*a*) and on a logarithmic scale (*b*). The strength of a fibre texture in the fibre pole is preferably specified in intensity units of m.r.d., *i.e.* multiples of the random distribution (Bunge, 1982; Chateigner, 2005). Applying a distribution function of the type given in equation (8) has the advantage that the parameter n directly corresponds to the m.r.d. value.

The effect of the thin-film absorption factor $A(t)$ on the $\cos^n\psi$ distribution is shown in Fig. 5 for n = 12 and some typical μt products. It can be seen from this plot that the decrease of μt causes a steady damping of intensity, comparable with the effect of temperature on a Bragg peak *via* the Debye–Waller factor.

The fact that the normalization constant N may be specified analytically for the $\cos^n\psi$ distribution is particularly helpful in the further development of an apparatus to describe fibre texture gradients. Of course, the other distribution functions

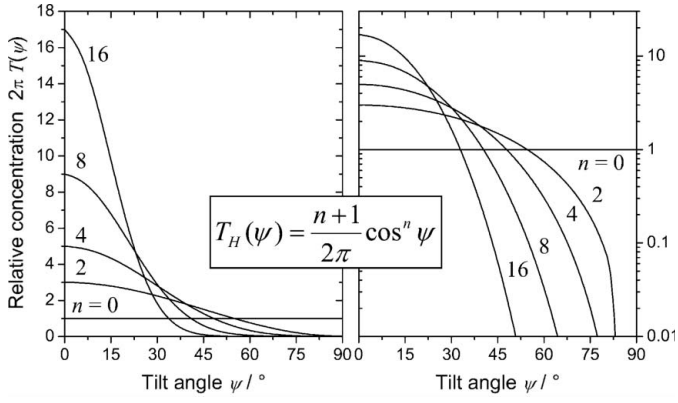

Figure 4
Plot of fibre texture model distribution functions $2\pi N_n \cos^n\psi$ for linear (left) and logarithmic ordinate (right).

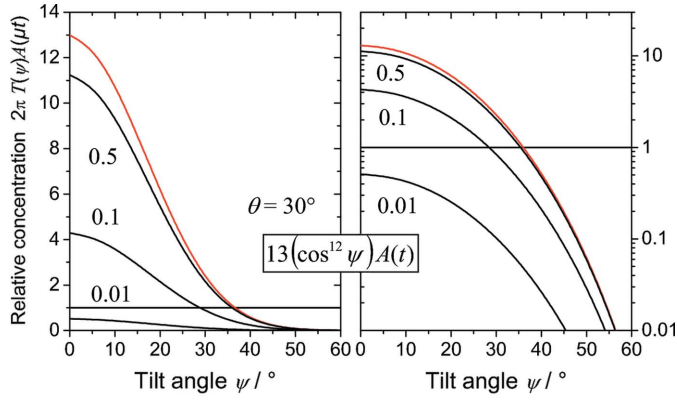

Figure 5
Effect of the absorption factor $A(t)$, equation (4), on the course of $2\pi N_n \cos^n\psi$ for n = 12 and a set of typical μt products; linear (left) and logarithmic scale (right). The red line in both plots stands for $A(t) = 1$, *i.e.* it is valid in the limit of $\mu t \rightarrow \infty$.

[1] According to the acknowledgement given in this paper, the naming of $T(y, r, G)$ as the March–Oertel–Dollase function would also appear appropriate.

are equally allowed. To use them, the normalization constant has to be evaluated numerically. In the following, however, use will only be made of the $N_n\cos^n\psi$ function to account for $T_H(\psi)$. This might be justified by the fact that with the present state of knowledge, no physical theory is at hand that prefers one texture distribution function over the other to model the evolution of texture during thin-film growth. The expression for the tilt-angle-dependent intensity of a fibre-texture Bragg reflection then becomes

$$I_H(\psi, t) = \mathrm{SCF}\,\lambda^3\,\mathrm{Lp}\,m_H\,|F_H|^2\,\frac{n+1}{2\pi}\cos^n\psi\,\frac{1}{2\mu}\,A(t). \quad (10)$$

To summarize this section, it may be stated that the dependency of tilt angle ψ on a fibre texture intensity distribution $I_H(\psi, t)$ is buried within the fibre orientation distribution $T_H(\psi)$ and, *via* the configuration parameter k, within the absorption factor $A(t)$.

3. Average information depth

The penetration depth τ of an X-ray beam into the sample is governed by the linear attenuation coefficient μ and the experimental geometry accounted for by the configuration factor k. For the case of an infinitely thick powder sample, the penetration depth from which the structural information stems in a Bragg reflection scales with $(\mu k)^{-1}$. For a thin film, however, the thickness t may become smaller than $1/\mu$, which would allow a part of the beam to traverse the sample fully without being scattered. Then, the introduction of an average information depth is more appropriate, accounting for the average depth from which the scattered X-ray beam stems (Birkholz, 2006). In the tilted Euler cradle configuration considered here (Figs. 1*a* and 1*b*) the average information depth $\bar{\tau}$ of a thin-film Bragg peak is given by

$$\bar{\tau} = \frac{\int_0^t z\exp(-\mu z k)\,\mathrm{d}z}{\int_0^t \exp(-\mu z k)\,\mathrm{d}z}. \quad (11)$$

The expression is easily solved to yield

$$\bar{\tau} = t\left[\frac{1}{\mu t k} + \frac{1}{1-\exp(\mu t k)}\right]. \quad (12)$$

In powder diffraction, the illuminated scattering volume is only restricted by the damping of the X-ray beam for any beam incidence. In this case, the first summand in equation (12) alone would correctly account for the information depth and would give the t-independent expression $(\mu k)^{-1}$. In thin-film diffraction, the second term on the right-hand side of equation (12) accounts for the geometrical truncation of the scattering volume. The physics of the equation can be understood by observing the limiting value for $\mu t \rightarrow 0$, yielding $\bar{\tau}$ as $t/2$. This mathematical limit stands for the case of an extremely thin film, where the scattered X-ray beam would almost equally stem from all parts of the sample. In this case, the average information depth $\bar{\tau}$ will tend to lie in the middle of the full layer $t/2$. In cases other than the limiting ones, however, the finite thickness of the sample and the diffractometer setting would principally yield scattering information from different depths. In any case, the average information depth is always limited by half the sample thickness, $\bar{\tau} \leq t/2$.

The important conclusion to be drawn from these considerations is that the fibre texture intensity $I_H(\psi)$ generally stems from different depths of the sample. A texture gradient may thus severely complicate the determination of the orientation distribution T_H from I_H. Bonarski *et al.* (1998) emphasized this point by stating that a pole figure, represented by $I_H(\psi)$ in the case considered here, becomes inconsistent in itself. It will be shown in the following section how consistency can be re-established and how the effect may be dealt with.

4. Fibre texture gradients

The gradation of texture will cause the texture distribution $T_h(\psi)$ to become a depth-dependent function $T_h(\psi, z)$. The situation is visualized in Fig. 6, where for each depth z a distinct orientation distribution T_h has been assigned to individual layers. An important constraint to any model of texture gradient is that a normalization condition comparable to equation (6) should hold. This means that for any arbitrary depth z the integral over $T_h(\psi, z)$ should yield the constant result

$$\int_0^{\pi/2} \left[T_h(\psi, z)\right]_{z=\mathrm{const}} \sin\psi\,\mathrm{d}\psi = \frac{1}{2\pi}. \quad (13)$$

This condition has to be included in the model functions introduced in the first section. The most simple texture gradient would be a linear one, where the texture-determining parameter only depends linearly on film depth z. Of the various distribution functions, the $N_n\cos^n\psi$ distribution appears well suited, because it allows for an analytical solution of a forthcoming integration. Performing a linear expansion of the order parameter $n \rightarrow n_0 + n_1 z$, the following depth-dependent fibre texture distribution function is obtained:

$$T_H(\psi, z) = \frac{n_0 + n_1 z + 1}{2\pi}\cos^{n_0+n_1 z}\psi. \quad (14)$$

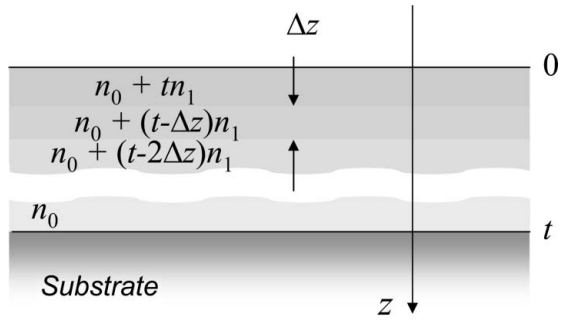

Figure 6
Model architecture of a thin film with a non-homogeneous degree $n = n_0 + n_1 z$ of fibre texture. The complete film is composed of individual layers at different height z that exhibit a linearly increasing degree of texture.

This expression is consistent with the generalized normalization condition [equation (13)]. The physical meaning of n_1 is simply that of texture gradient, to be specified per unit thickness, and thus compares with the dimension of the linear attenuation coefficient μ. The parameter n_0 stands for the initial texture strength. That means that n_0 does not necessarily indicate the texture strength at the interface to the substrate, but at a height level that appears, due to experimental constraints like attenuation coefficient and sample thickness, as horizon to the X-ray probe. Now we have to turn to the generalization of the integral intensity formulae [equation (5)] for the case of a graded texture.

The kinematic intensity of a Bragg peak was shown in equation (5) to scale with the product of texture factor $T_\mathrm{h}(\psi)$ and scattering volume V_sc. The physical meaning behind the mathematical operation is that only those parts of the scattering volume have to be considered for which the orientation distribution is such that they scatter into the detector. For a polycrystalline thin film exhibiting a texture variation on the length scale of its inverse X-ray attenuation coefficient μ, the formula for the integral intensity of Bragg reflection, equation (5), is not valid, but deserves a generalization. It is the product of texture coefficient $T_\mathrm{h}(\psi)$ and absorption factor $A(t)$ that has to be subjected to change. In the derivation of equation (5), the absorption coefficient is obtained from the integration over scattering events in the irradiated volume. If the infinitesimal elements of the scattering volume are not randomly, but to a certain extent preferentially oriented, the integration has to be weighted by a measure specifying the degree of preferred orientation, *i.e.* by the texture distribution. Since this work is concerned with depth variations of texture, only z variations of texture distributions have to be considered, and the weighting terms are of the form $T_\mathrm{h}(\psi, z)$. Instead of the product of T_H and $A(t)$, the integration over all beam paths has to include the texture distribution and it has to be generalized by substituting

$$T_\mathrm{h}(\psi)\,\frac{1}{2\mu}\,A(t) \;\rightarrow\; \int_0^{\ell_\mathrm{max}} T_\mathrm{h}(\psi, z)\exp(-2\mu\ell)\,\mathrm{d}\ell = \frac{k}{2}\int_0^t T_\mathrm{h}(\psi, z)\exp(-\mu z k)\,\mathrm{d}z. \quad (15)$$

The integration has to be carried out over the full depth of the illuminated sample, restricted either by the film thickness or by the damping of the incoming X-ray beam. The decisive integration step may be considered as a finite Laplace transformation and we may abbreviate

$$L^t\big[T_\mathrm{h}(\psi, z)\big] = \int_0^t T_\mathrm{h}(\psi, z)\exp(-\mu z k)\;\mathrm{d}z. \quad (16)$$

The integral intensity from a Bragg reflection may finally be expressed by

$$I_\mathrm{h}(\psi, t) = \mathrm{SCF}\,\lambda^3\,\mathrm{Lp}\,\big|F_\mathrm{h}\big|^2\,m_\mathrm{h}\,\frac{k}{2}\,L^t(T_\mathrm{h}). \quad (17)$$

This is the fundamental equation to describe the intensity distribution of a depth-dependent fibre texture in a thin film. It directly represents the experimental result that is obtained by the thin-film diffractionist, when measuring the intensity as a function of tilt. Obviously, this is a rather complex expression and it seems that texture gradients in thin films, in spite of their almost universal occurrence, have so far not been derived by analysing the intensity distribution within the framework of this equation.

For an application of the approach, the texture distribution functions given in the first section have to be inserted into equation (16) and the measured intensities have to be subjected to a numerical regression. Additional fitting parameters that account for the variation of texture within the sample have to be included in the distribution function. Performing the finite Laplace transformation to the gradient $N_n\cos^n\psi$ distribution given in equation (14) is intriguing, since it allows the illustration of some interesting effects associated with fibre texture gradients in thin films that are of general validity. The task then becomes to solve for

$$\frac{k}{4\pi}\int_0^t (n_0 + n_1 z + 1)\big(\cos^{n_0+n_1 z}\psi\big)\exp(-\mu z k)\,\mathrm{d}z. \quad (18)$$

The integration is preferably performed by decomposing the integral kernel into two summands and by introducing the parameter

$$M = \mu k - n_1\ln(\cos\psi), \quad (19)$$

yielding the intermediate result

$$\frac{k}{4\pi}\cos^{n_0}\psi\left[(n_0+1)\int_0^t \exp(-Mz)\,\mathrm{d}z + n_1\int_0^t z\exp(-Mz)\,\mathrm{d}z\right] \quad (20)$$

and the solution

$$\frac{k}{2}L^t(T_\mathrm{h}) = \frac{1}{2\pi}\left\{n_0 + n_1 t\left[\frac{1}{Mt} + \frac{1}{1-\exp(Mt)}\right] + 1\right\} \times \cos^{n_0}\psi\,\frac{1-\exp(-Mt)}{2M/k}. \quad (21)$$

Introducing the abbreviations for the modified absorption factor

$$\tilde{A}(t) = 1 - \exp(-Mt) = 1 - (\cos^{n_1 t}\psi)\exp(-\mu t k), \quad (22)$$

and the modified normalization factor

$$\tilde{N} = \frac{1}{2\pi}\left\{n_0 + n_1 t\left[\frac{1}{Mt} + \frac{1}{1-\exp(Mt)}\right] + 1\right\}, \quad (23)$$

the formulae for the depth-graded texture intensity with an essentially $\cos^n\psi$ fibre distribution function finally becomes

$$I_\mathrm{H}(\psi, t) = \mathrm{SCF}\,\lambda^3\,\mathrm{Lp}\,m_\mathrm{H}\,\big|F_\mathrm{H}\big|^2\,\tilde{N}\cos^{n_0}\psi\,\frac{k}{2M}\,\tilde{A}(t). \quad (24)$$

In this form, the close relationship with equation (10) can be realised, although significant differences have to be stated when equation (24) is compared with the gradient-free expression. Most relevant, both $\tilde{A}(t)$ and $\tilde{N}$ depend on the texture gradient n_1. For other texture distribution functions, the expression will of course become different. It is a clear advantage of the $\cos^n\psi$ distribution, however, that it allows for an analytical solution of equation (17), since some basic conclusions may be drawn that are of more general validity.

First of all, the limiting value for zero tilt angles is of interest. For this case of $\psi = 0$ or $\cos\psi = 1$, the M factor limit yields the product of the attenuation and the configuration factor

$$\lim_{\psi\to 0} M = \mu k = \frac{2\mu}{\sin\theta}. \tag{25}$$

Furthermore, the proportional constant of the n_1 term in the modified normalization factor, equation (23), can be realised to give the average information depth $\bar{\tau}$ from equation (12) for vanishing tilt. We end up with the an intensity for zero tilt of

$$\lim_{\psi\to 0} I_{\rm H}(\psi, t) = {\rm SCF}\,\lambda^3\,{\rm Lp}\,m_{\rm H}\left|F_{\rm H}\right|^2\left(\frac{n_0 + n_1\bar{\tau} + 1}{2\pi}\right)\frac{A(t)}{2\mu}. \tag{26}$$

It states that the intensity in the pole ($\psi = 0$) is not proportional to $n_0 + 1$, but proportional to this term plus the product of the gradient multiplied by the average information depth, $n_1\bar{\tau}$. This is the reflection intensity measured in a coplanar $\theta/2\theta$ scan and appears a very reliable result from a physical point of view.

A second interesting point of equation (24) is related to the position of maximum intensity. It has to be emphasized again that only fibre textures are considered here with the fibre axis in direction of the substrate normal. This means that the highest concentration of lattice planes with an orientation parallel to the substrate plane occurs for zero tilt. Consequently, the highest intensity can be expected to arise at $\psi = 0$, which appears self-evident when modelling the texture by a $\cos^n\psi$ or any other distribution given in the first section.

It may be realised from equation (24), however, that the course of $I_{\rm H}$ depends on the product of two monotonic functions, $\cos^{n_0}\psi$ and $\tilde{A}(t)$, of opposing tendencies. Whereas $\cos^{n_0}\psi$ is monotonically decreasing for increasing tilt, $\tilde{A}(t)$ follows the opposite trend. Since both factors enter the intensity formulae [equation (24)], the course of $I_{\rm H}(\psi, t)$ will depend on the balance between n_0 and $n_1 t$ on the one hand and μt on the other hand. Some plots of the product functions for the ungraded and for the graded texture case, $A(t)\cos^n\psi$ and $\tilde{A}(t)\cos^{n_0}\psi$, are given in Fig. 7(*a*) for reliable parameters to demonstrate the effect ($n_1 t = 8$ and $n_0 = 10$ or $n = 10$, respectively). It can be seen that for certain parameter values, the product function $\tilde{A}(t)\cos^{n_0}\psi$ takes its maximum at positions distinct from $\psi = 0$, and so will the measured intensity. For the last two functions with $\mu t/\sin\theta = 0.2$, the two-dimensional intensity pole figures as usually measured over the (ϕ, ψ) plane are also schematically given in Fig. 7(*b*). A characteristic ring of maximum intensity is seen to surround the origin. Such a pattern is comparable with that of an asymmetric reflection and may falsely imply that the fibre pole differs from the $\psi = 0$ position.

Obtaining such a result may lead to the misinterpretation that the fibre axis is inclined with respect to $\mathbf{s}_3$. The physical meaning behind the effect is due to the balance between texture gradient and average information depth. Since $\bar{\tau}$ varies with varying tilt angle ψ, different depths are probed during the course of the measurement, with regions closer to the film surface being probed for higher ψ values. For a positive texture gradient, as is usually observed in thin polycrystalline films, sample regions with a higher degree of texture may mimic a higher concentration of lattice planes for non-zero tilt. From a mathematical point of view, this is caused by the modulation of the $\exp(-\mu t k)$ term by the $\cos^{n_1 t}\psi$ factor in equation (22). The latter term is missing in the conventional absorption factor $A(t)$ [see equation (4)] and the effect of the shifted intensity maximum will not be observed for an ungraded fibre texture. The observation of a maximum intensity apart from $\psi = 0$ in $I_{\rm H}(\psi, t)$ can thus be taken as a strong hint that the sample exhibits a texture gradient. It is evident from equations (19) to (24) that the effect will depend on the relative strength of the μt and $n_1 t$ products.

Regarding the experimental determination of texture gradients, it might become difficult to measure the magnitude of n_1 or $n_1 t$, in particular, if monotonically decreasing intensity distributions $I_{\rm H}(\psi, t)$ are observed and if the experiment relies on an irrevocable μt product. In the majority of studies, where a gradient was endeavoured of being quantified, a series of samples of varying thickness t_i was prepared and the fibre texture was measured in each sample separately (see for instance: Kamiya *et al.*, 1999; Birkholz *et al.*, 2000; Saerens *et al.*, 2000; Shin *et al.*, 2002; Birkholz *et al.*, 2003; Fenske *et al.*, 2005). The texture strength or the degree n could then be specified as a function of average information depth $\bar{\tau}_i$ of the different samples and the gradient could be determined from the plot of $n(\bar{\tau}_i)$ or its inverse Laplace transform.

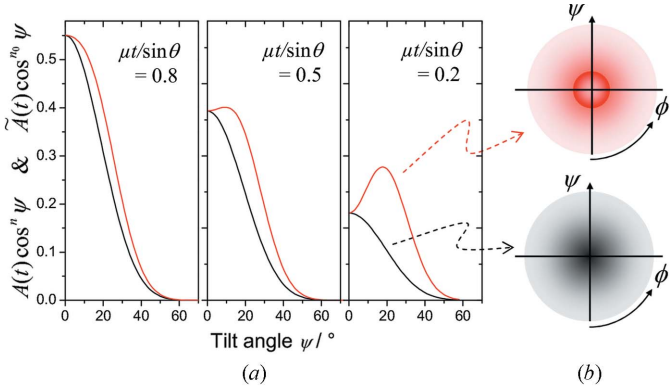

Figure 7
(*a*) Plots of $A(t)\cos^{10}\psi$ according to equation (4), as black lines, and $\tilde{A}(t)\cos^{10}\psi$ with $n_1 t = 8$ according to equation (22), as red lines. Both curves in each box obey the same $\mu t/\sin\theta$ as indicated in the inset. (*b*) From the last two curves, schematic pole-figure plots $I_{\rm H}(\phi, \psi)$ are displayed on the right with increasing intensity symbolized by the strength of the ring colours.

An alternative approach to the quantitative determination of n_1 can be drawn from Fig. 2, where the μt products of different thin-film materials are presented. It is realised from this plot that μt and therefore also the ratio of μt over $n_1 t$ is subjected to strong variations for beam energies below and above elemental absorption edges. For ZnO, for instance, μt varies by about an order of magnitude between $E = 8$ and 10 keV. The recording of $I_H(\psi, t)$ distributions with different energies would thus probe the sample at different depths. Accordingly, the use of various wavelengths offers an approach to determine the magnitude of a fibre texture gradient within one single specimen, *i.e.* without using a thickness series of samples. First results of this approach will be presented in a forthcoming work (Birkholz *et al.*, 2007).

5. Conclusions

In conclusion, it has been shown how a texture gradient in a polycrystalline thin film would affect the intensity distribution $I_h(\psi, t)$ of the fibre texture reflection measured as a function of tilt angle. Although the focus was on the measurements in the Ψ mode, the formalism may equally be applied for measurements in the Ω configuration. Vaudin has shown how the $T_H(\psi, t)$ function can be extracted from the measured intensity function $I_H(\omega, t)$ (Vaudin *et al.*, 1998).

The presented concept is rather general and may be applied whenever the finite Laplace transform of the texture distribution may be deconvoluted from the experimental intensity [equation (17)]. The derived equations allow for the modelling of not only graded texture distributions, but inhomogeneous fibre texture distributions $T_H(\psi, z)$ in general. Furthermore, polycrystalline samples other than thin films may be analysed in the presented framework by calculating the limits of appropriate formulae for $\mu t \rightarrow \infty$.

The quantitative determination of texture gradients will probably find its main application in the study of thin-film growth. For instance, the evolution of texture and other microstructural properties has frequently been assigned to the variation of residual stress with increasing film thickness. The combined analysis that now becomes possible for both residual stress and texture gradients will allow a comparison of both phenomena and may thus facilitate our understanding of the mechanisms of thin-film growth.

I wish to thank Daniel Chateigner, Nora Darowski, Christoph Genzel, Peter Zaumseil and Ivo Zizak for helpful discussions.

References

Almer, J., Lienert, U., Peng, R. L., Schlauer, C. & Odén, M. (2003). *J. Appl. Phys.* **94**, 697–702.

Baron, H. U. & Hauk, V. (1988). *Z. Metallkd.* **79**, 127–131.

Birkholz, M. (2006). *Thin Film Analysis by X-ray Scattering*, ch. 1, 4, 5. Weinheim: Wiley-VCH. (ISBN3-527-31052-5.)

Birkholz, M., Darowski, N. & Zizak, I. (2007). Submitted.

Birkholz, M., Genzel, C. & Jung, T. (2004). *J. Appl. Phys.* **96**, 7202–7211.

Birkholz, M., Selle, B., Conrad, E., Lips, K. & Fuhs, W. (2000). *J. Appl. Phys.* **88**, 4376–4379.

Birkholz, M., Selle, B., Fenske, F. & Fuhs, W. (2003). *Phys. Rev. B*, **68**, 205414.

Bonarski, J. T., Bunge, H. J., Wcislak, L. & Pawlik, K. (1998). *Textures Microstruct.* **31**, 21–41.

Bunge, H.-J. (1969). *Mathematische Methoden der Texturanalyse*. Berlin: Akademie-Verlag.

Bunge, H.-J. (1982). *Texture Analysis in Materials Science*. London: Butterworth.

Caliendo, C. & Imperatori, P. (2004). *J. Appl. Phys.* **96**, 2610–2615.

Chateigner, D. (2000). *Analyse de Texture Quantitative: un outil d'interpretation des propriétés anisotropes entre poudre et monocristal*, l'Habilitation à Diriger des Recherches, Universite du Maine, Le Mans.

Chateigner, D. (2005). *Combined Analysis: Structure-texture-microstructure-phase-stresses-reflectivity determination by X-ray and neutron scattering*, http://www.ecole.ensicaen.fr/~chateign/texture/combined.pdf.

Dollase, W. A. (1986). *J. Appl. Cryst.* **19**, 267–272.

Dong, L. & Srolovitz, D. J. (1999). *Appl. Phys. Lett.* **75**, 584–586.

Drift, A. van der (1967). *Philips Res. Rep.* **22**, 267–288.

Fenske, F., Selle, B. & Birkholz, M. (2005). *J. Appl. Phys. Jpn*, **44**, L662–L664.

Fujimura, N., Nishihara, T., Goto, S., Xu, J. & Ito, T. (1993). *J. Cryst. Growth*, **130**, 269–279.

Genzel, C. (1998). *Phys. Status Solidi A*, **165**, 347–360.

Genzel, C. (1999). *J. Appl. Cryst.* **32**, 770–778.

Genzel, C. (2004). *Problems Related to X-ray Stress Analysis in Thin Films in the Presence of Gradients and Texture, Diffraction Analysis of the Microstructure of Materials*, edited by E. J. Mittemeijer & P. Scardi, pp. 473–503. Berlin: Springer.

Genzel, C., Broda, M., Dantz, D. & Reimers, W. (1999). *J. Appl. Cryst.* **32**, 779–787.

Genzel, C. & Reimers, W. (1998). *Phys. Status Solidi. A*, **166**, 751–762.

Genzel, C. & Reimers, W. (2003). *Z. Metallkd.* **94**, 655–661.

Göbel, T., Menzel, S., Hecker, M., Brückner, W., Wetzig, K. & Genzel, C. (2001). *Surf. Coat. Technol.* **142–144**, 861–867.

Kajikawa, Y. (2006). *J. Cryst. Growth*, **289**, 387–394.

Kajikawa, Y., Noda, S. & Komiyama, H. (2003). *J. Vac. Sci. Technol. A*, **21**, 1943–1954.

Kamiya, T., Nakahata, K., Miida, A, Fortmann, C. M. & Shimizu, I. (1999). *Thin Solid. Films*, **337**, 18–22.

Knuyt, G., Quaeyhaegens, C., D'Haen, J. & Stals, L. M. (1996). *Phys. Status Solidi B*, **195**, 179–193.

Lutterotti, L., Chateigner, D., Ferrari, S. & Ricote, J. (2004). *Thin Solid Films*, **450**, 34–41.

March, A. (1932). *Z. Kristallogr.* **81**, 285–297.

Ohring, M. (2002). *The Materials Science of Thin Films*, 2nd ed. San Diego: Academic Press.

Pelleg, J., Zevin, L. Z., Lungo, S. & Croitoru, N. (1991). *Thin Solid Films*, **197**, 117–128.

Platt, C. L., Wiermann, K. W., Svedberg, E. B., van de Veerdonk, R., Howard, J. K., Roy, A. G. & Laughlin, D. E. (2002). *J. Appl. Phys.* **92**, 6104–6109.

Popa, N. C. & Balzar, D. (2001). *J. Appl. Cryst.* **34**, 187–195.

Rauschenbach, B. & Helming, K. (1989). *Nucl. Instrum. Methods B*, **42**, 216–223.

Saerens, A., Van Houtte, P., Meert, B. & Quaeyhaegens, C. (2000). *J. Appl. Cryst.* **33**, 312–322.

Scardi, P. & Dong, Y. H. (2001). *J. Mater. Res.* **16**, 233–242.

Shin, C.-S., Gall, D., Kim, Y.-W., Hellgren, N., Petrov, I. & Greene, E. (2002). *J. Appl. Phys.* **92**, 5084–5093.

Vaudin, M. D., Rupich, M. W., Jowett, M., Riley, G. N. & Bingert, J. F. (1998). *J. Mater. Res.* **13**, 2910–2919.

Welzel, U. & Mittemeijer, E. J. (2003). *J. Appl. Phys.* **93**, 9001–9011.

Wenk, H.-R., Sintubin, M., Huang, J., Johnson, G. C. & Howe, R. T. (1990). *J. Appl. Phys.* **67**, 572–574.

Wenk, H.-R. & van Houtte, P. (2004). *Rep. Prog. Phys.* **67**, 1367–1428.